ELSEVIER

International Journal of Heat and Fluid Flow 23 (2002) 222–231

International Journal of HEAT AND FLUID FLOW

www.elsevier.com/locate/ijhff

Computational modeling of flow and heat transfer in industrial applications ☆

Suhas V. Patankar *

Department of Mechanical Engineering, University of Minnesota, Minneapolis, MN 55455, USA
Innovative Research, Inc., Plymouth, MN 55447, USA

Abstract

This paper presents application of computational modeling to four problems of industrial importance. The problems include ventilation and fire spread in highway tunnels, chemical vapor infiltration for manufacturing fiber-reinforced composites, refining hearths used for elimination of impurities in high-performance alloys, and the transport processes in a cement kiln. The noteworthy physical and computational features of each problem are described and some selected results are shown along with comparison with measurements. © 2002 Published by Elsevier Science Inc.

1. Introduction

Over the last 25 years, computational fluid dynamics and heat transfer have been increasingly used for a wide variety of engineering applications. In the beginning, the use of these techniques was customary only in the aerospace and nuclear fields. Subsequently, the use has spread to a variety of products, physical situations, and manufacturing processes. Some examples of interesting applications of computational modeling are cooling of electronics systems, rotating and reciprocating machinery, furnaces and combustion chambers, chemical vapor deposition, plasma processing, refining hearths for alloys, and grain drying.

In such applications, computational modeling allows us to perform simulations of complex problems, investigate the effect of different design parameters, obtain detailed distributions of all relevant variables, and gain insight into the underlying physical processes. By a proper use of modeling, one can cut down on time-consuming and costly experiments and field measurements, avoid design by trial and error, obtain speedy results, and design better products and processes.

Today's computers and computational techniques make it possible to include a very detailed representation of the problem and a comprehensive set of models for the relevant physical processes. However, it is often desirable to use some approximations and idealizations to reduce the computational expense. Then, computational modeling can be used in a *routine* manner in engineering design.

The purpose of this paper is to describe four selected applications of computational fluid dynamics and heat transfer to problems of industrial interest. In each case, the computational novelties are briefly outlined and some of the interesting results are presented. The four applications also illustrate the use of appropriate simplifications adopted for computational efficiency.

The first problem deals with ventilation and fire spread in highway tunnels. It shows the validation of a computational model of modest complexity by comparison with extensive field measurements. The next problem deals with chemical vapor infiltration (CVI) used for manufacturing fiber-reinforced composites. This problem presents a number of computational challenges. An interesting combination of models at the microscopic and macroscopic levels is used to address the problem without requiring excessive computing resources. The third problem involves refining hearths used for elimination of impurities in high-performance alloys. The computational model incorporates buoyancy and Marangoni forces, melting/freezing, and particle

☆ This paper is a revised and expanded version of a paper presented at CHT'01, the Second International Symposium on Advances in Computational Heat Transfer (Palm Cove, Qld., Australia, 20–25 May 2001), the proceedings of which were published by Begell House, Inc.

* Tel.: +1-763-519-0105; fax: +1-763-519-0239.
E-mail address: patankar@inres.com (S.V. Patankar).

0142-727X/02/$ - see front matter © 2002 Published by Elsevier Science Inc.
PII: S0142-727X(02)00170-4

tracking. Finally, the modeling of the transport processes in a cement kiln is described.

2. Tunnel ventilation

2.1. The problem considered

Fire spread, smoke movement, and ventilation in highway tunnels is an important problem of public safety. One approach for blowing the smoke out of the tunnel is to create a longitudinal flow using jets fans. Since measurements from an extensive test program conducted on Memorial Tunnel were available (Massachusetts Highway Department, 1995), a computational model was constructed and validated against the test data. This study is described in Karki et al. (2000a,b) (see also Massachusetts Highway Department, 1999); also, additional details are available on www.tunnelfire.com.

2.2. The computational model

The computations are based on the solution of three-dimensional equations for flow, temperature, and smoke concentration. The turbulence is handled by the k–ε model with appropriate source terms for turbulence production due to buoyancy. The fire is represented as a source of heat and mass, distributed in a region attributed to the fire. The same region also serves as a source of smoke concentration.

Jet fans are mounted on the ceiling of the tunnel as shown in Fig. 1. They are treated as volumetric flow devices and are modeled by appropriate sources and sinks of mass and momentum. The air jet issued by a jet fan entrains surrounding air and produces a much larger longitudinal flow through the tunnel to drive the smoke out of the tunnel.

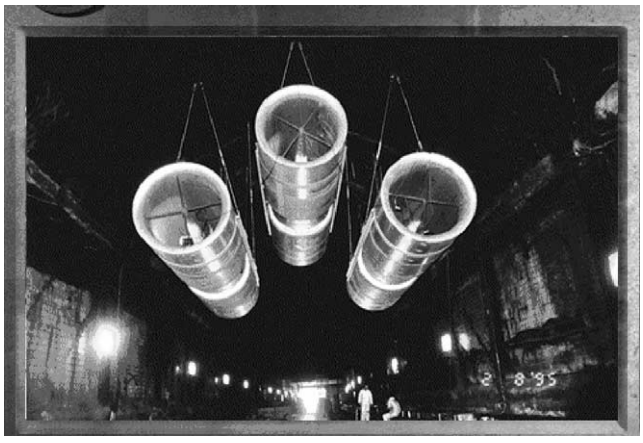

Fig. 1. Jet fans mounted in the tunnel.

The sample results included in this paper pertain to the case of a 100 MW fire. Three minutes after the ignition, six jet fans were activated and maintained for 12 min; thereafter, one jet fan was deactivated.

2.3. Results for bulk flow

The total flow rate at two different longitudinal locations is plotted as a function of time in Fig. 2. The flow rate changes due to the buoyancy forces and the effect of the jet fans. The computed solution agrees very well with the measurements.

2.4. Distribution of temperature and smoke concentration

Figs. 3–5 show the contours of temperature and smoke distribution at three important instants in the process of fire spread and ventilation. Each figure includes the computed and measured temperature contours followed by the computed and measured *visibility* contours. Visibility is derived from the smoke concentration by using

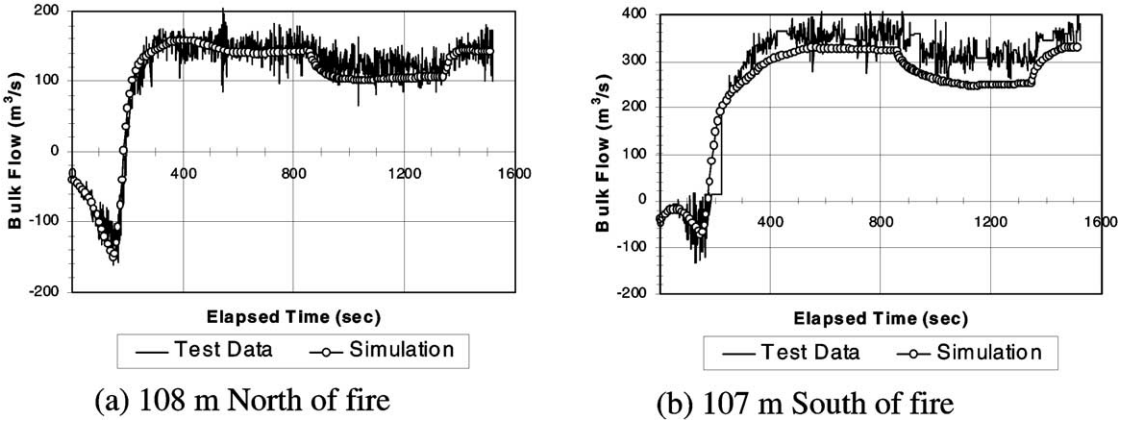

Fig. 2. Total flow rate through the tunnel as a function of time.

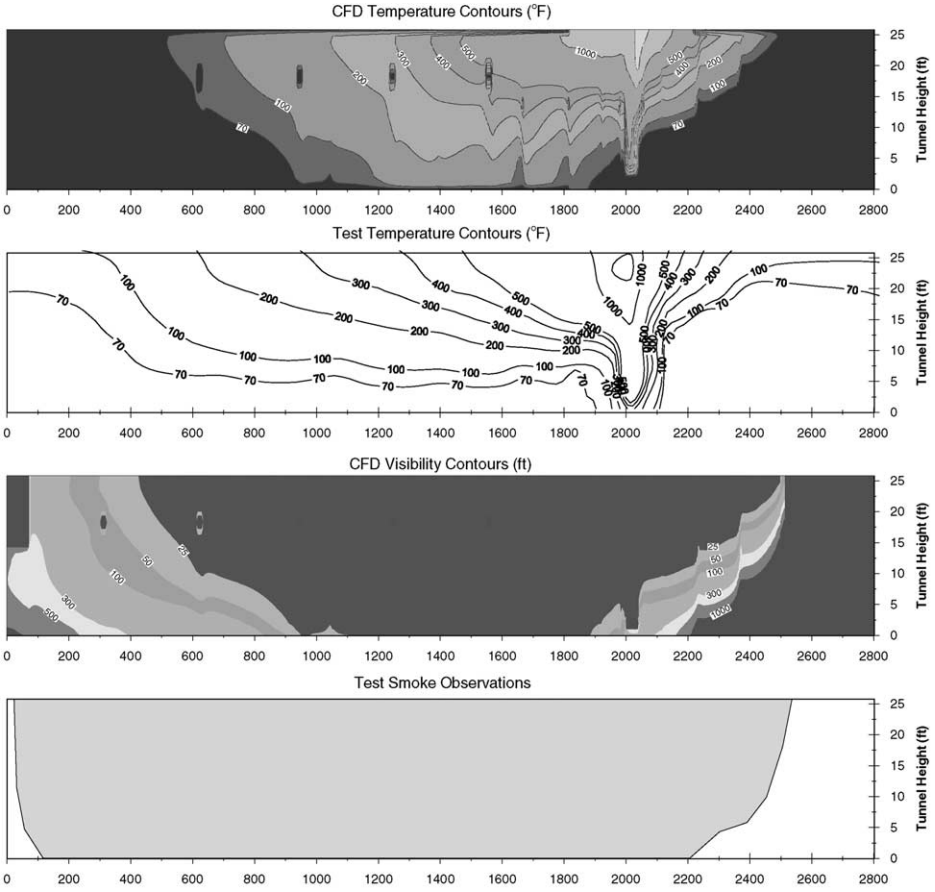

Fig. 3. Distribution of temperature and smoke concentration at $t = 147$ s (no jet fans on).

an empirical relation. The *measured* visibility contours are based on whether the video cameras placed in different locations were able to "see" anything or not.

Fig. 3 displays the condition before any jet fans are switched on. Because of a slight gradient in the tunnel, the fire and smoke preferentially move towards the left (north) end of the tunnel. Within about 2 min, nearly the whole tunnel is filled with smoke. When the six jet fans are activated, they push the smoke out of the right (south) end of the tunnel. This condition is shown in Fig. 4. Fig. 5 refers to the condition when only five jet fans are operating; they are sufficient to keep the smoke out but there is some evidence of "back-layering", i.e., the spread of a smoke layer upstream of the fire location.

The results presented in Figs. 3–5 show a satisfactory agreement between the computation and measurement.

3. Chemical vapor infiltration

3.1. The manufacturing process

One possible method for building silicon–carbide fiber-matrix composites is to create a preform of layers of a fiber weave, pass a reactive gas such as CH_3SiCl_3 through the pores, and deposit silicon carbide on the fibers by a surface chemical reaction. This manufacturing process is called CVI. Whereas the process is capable of producing high-quality parts of final desired shapes, careful process control is needed. As the inter-fiber space gets filled up, the formation of inaccessible voids can lead to only partially densified material. Also, when large parts are made, a rapid densification at the outer boundaries can prevent any infiltration to the inner region.

3.2. The modeling challenge

The complete computational simulation of the CVI process presents the difficulty of two different scales. The fibers and the interspaces between them are only a few microns in size, while the finished parts may be many centimeters long. Further the process is time-dependent and the fibers grow with time due to deposition. Thus, to perform transient computations on the scale of the whole part while resolving the details around individual fibers of changing geometry is obviously beyond the reach of common computer resources. The problem

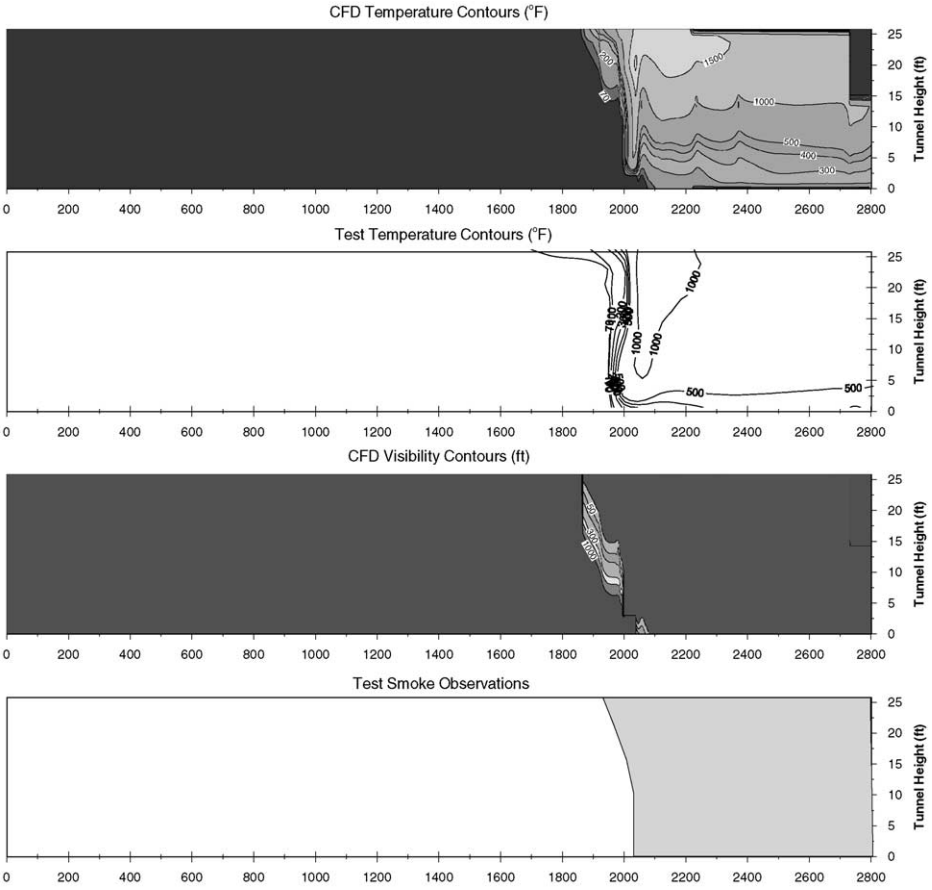

Fig. 4. Distribution of temperature and smoke concentration at $t = 700$ s (six jet fans on).

can, however, be simplified by considering micro- and macro-models and quasi-steady behavior as described below.

3.3. The micro-model

The main idea of this approach is to use the microscopic details of the fiber arrangements to characterize the *effective* properties of the resulting porous material and to calculate the deposition process in the whole part by using these properties. The fiber weaves are made like textile material with a regular fiber pattern. A typical weave is shown in Fig. 6. (The fibers do not seem to have a circular cross-section. Actually, they are fiber tows, which are bundles of many fibers. The resulting bundle may have an elliptical cross-section.) The regularity of the weave pattern allows the identification of a unit cell, shown in Fig. 7, such that by a repetition of the cell the entire preform can be constructed. We also need to consider unit cells at different levels of densification, when the fiber tows have grown to a larger size. These are also shown in Fig. 7, where ϕ denotes the solid volume fraction or the degree of densification.

A unit cell can be analyzed, with modest computational effort, to obtain the effective properties of the porous material. By imposing gradients of pressure, temperature, and concentration over the unit cell, we first calculate the fields of velocity, temperature, and concentration throughout the domain defined by the unit cell. This allows us to obtain the corresponding fluid flow rate, heat flow rate, and diffusion flux and thus evaluate the effective permeability, conductivity, and diffusion coefficient for the material. These properties can be anisotropic. Further, they need to be calculated for the geometries that correspond to different levels of densification as shown in Fig. 7. Representative results for the effective thermal conductivity are shown in Fig. 8 for a particular weave known as the 5-harness satin. The final outcome of the micro-calculation is a database of the effective properties for different weave geometries, different directions (anisotropy), and different levels of densification.

3.4. The macro-model

Once the porous material is characterized in this manner, the CVI process can be modeled for the actual

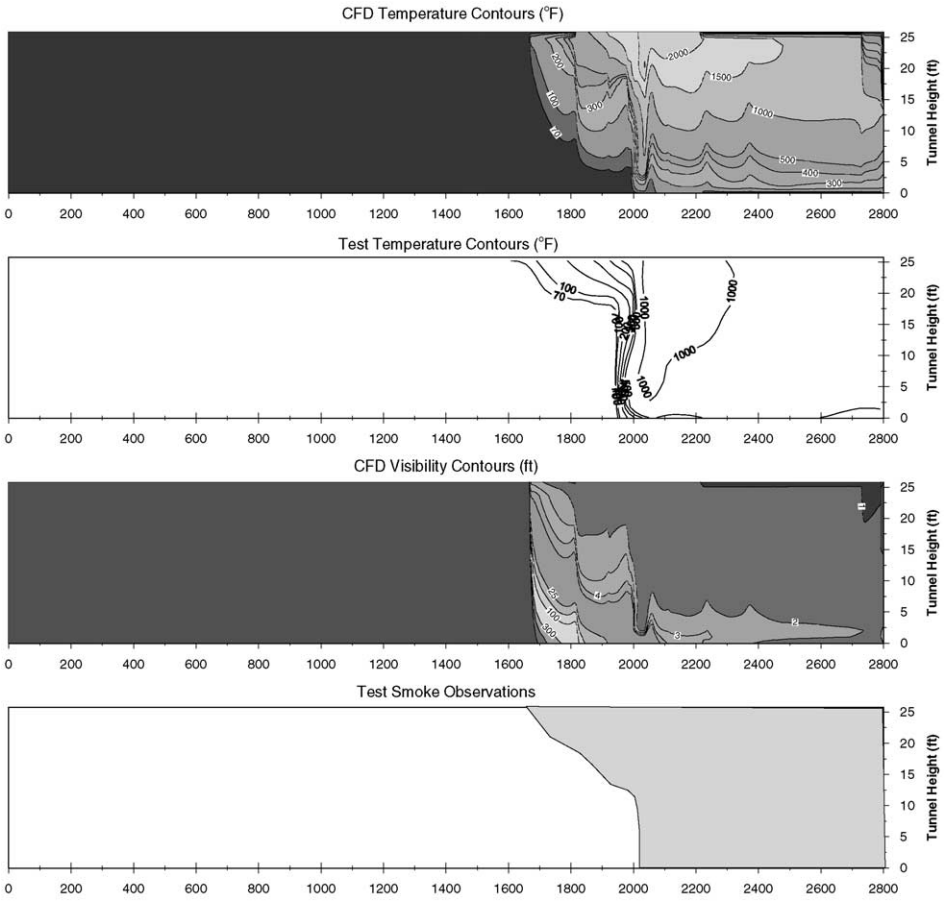

Fig. 5. Distribution of temperature and smoke concentration at $t = 1000$ s (five jet fans on).

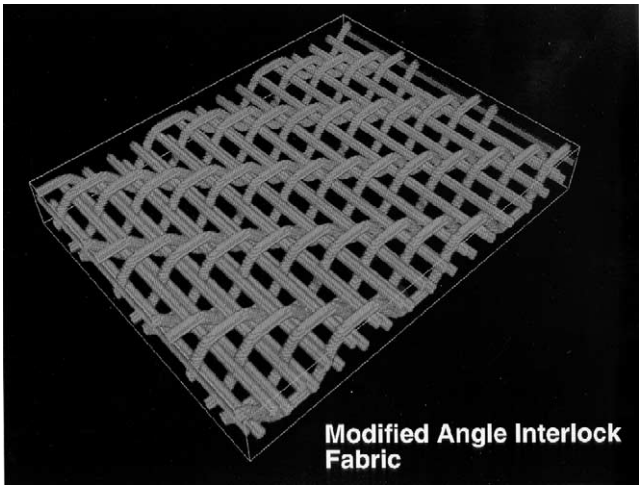

Fig. 6. A typical weave used for fiber preforms.

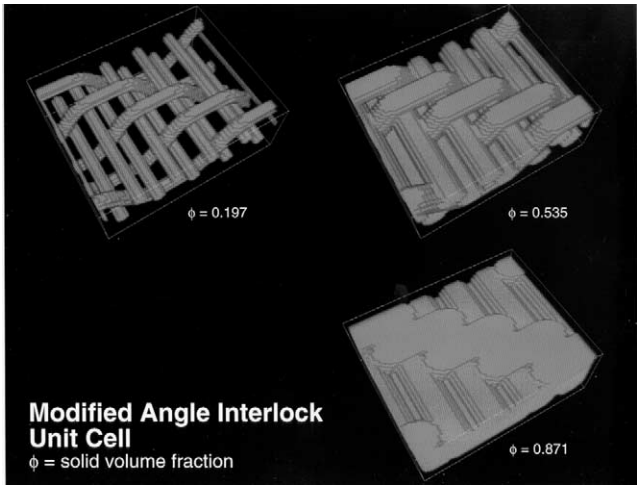

Fig. 7. Unit cells for the chosen weave at different densification levels.

dimensions of the preform (without using a grid resolution of the size of the fibers). Although the real process is transient, the growth of the fibers is very slow and thus allows a quasi-steady formulation. For the initial undensified preform, the steady-state distributions of fluid flow, temperature, and reactive-gas concentration can be calculated (based on the effective transport properties obtained in the micro-model). This solution gives the local deposition rate of silicon carbide (which is nonuniform due to variations in temperature and reactive-gas concentration). It is then used to find the local level of densification (i.e., the solid volume frac-

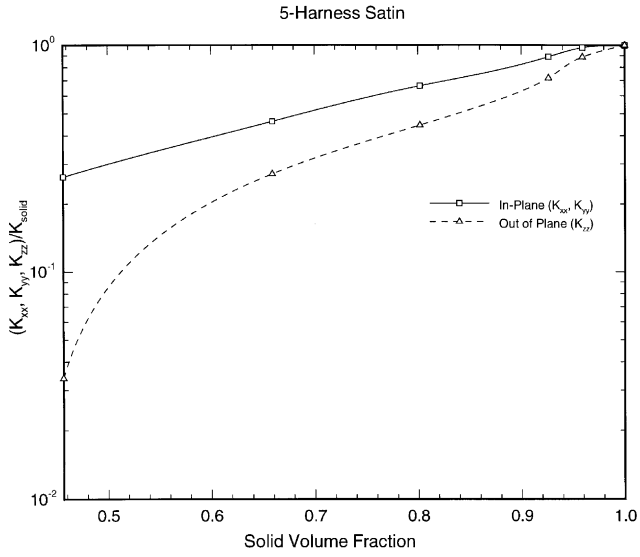

Fig. 8. Variation of effective thermal conductivity at different densification levels.

tion) after a finite time step. For this new geometry, another steady-state calculation is performed by using the *local* effective transport properties based on the local level of densification. The corresponding local deposition rates are used to advance the geometry to the next instant of time. Thus, through a succession of steady-state solutions, the progressive densification of the preform is predicted. The computation is continued until no further deposition can occur due to inaccessible voids or plugged boundaries.

3.5. Sample results

A simple application of the ideas described above is shown in Fig. 9 for a preform slab of certain thickness

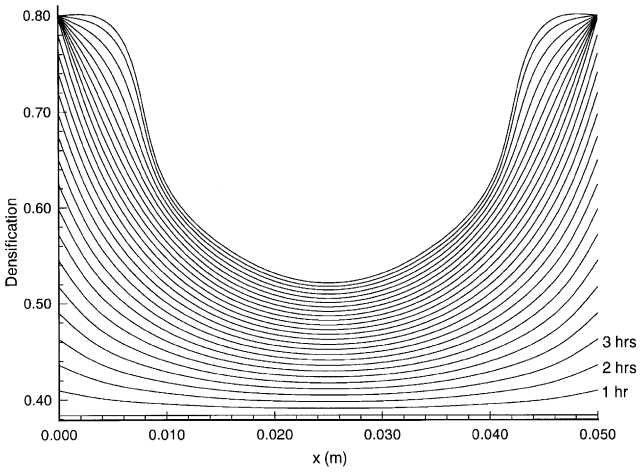

Fig. 9. Densification profiles in a preform slab.

exposed to the reactive gas on its both surfaces. The densification profiles shown in Fig. 9 for different instants of time indicate that, as the reactive gas infiltrates into the preform and its concentration gets depleted, much less deposition occurs in the interior region. The final result is that, after the inter-fiber spaces at the faces of the preform get plugged up, the CVI process stops leaving the interior insufficiently densified. Since the chemical reaction rate depends on temperature, thermal gradients can be used to encourage or discourage densification in different regions. Fig. 10 shows the case of a rectangular preform exposed to the reactive gas on one face and maintained at a higher temperature on the opposite face to encourage early deposition there. The progression of the temperature and concentration fronts with time is shown along with the amount of densification achieved at different locations. The results for even simple problems like these show the difficulty of obtaining a uniform densification everywhere. More

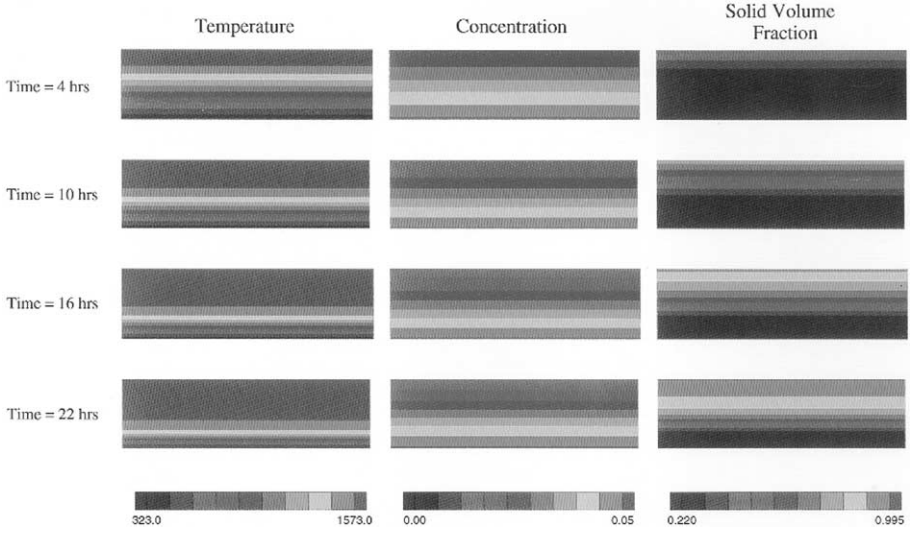

Fig. 10. Densification process with a thermal gradient.

interesting results have been obtained for complex geometries and boundary conditions, but are not shown here due to lack of space.

4. Refining hearth

4.1. Refining of high-performance alloys

Aircraft engine parts are made from titanium alloys that must be ultra-pure. When titanium reacts with nitrogen, hard particles of titanium nitride are formed. If they are embedded in an ingot of the alloy, these "inclusions" form a weak spot, which can lead to the failure of a critical engine part. Some of the airplane accidents have been traced back to the presence of a single hard inclusion in the turbine disk. For this reason, the alloys used for these critical applications are refined and re-refined to achieve ultimate purity. One arrangement for the refining process is to use a refining hearth setup as shown in Fig. 11. The unrefined material is first melted in a melting hearth, it then flows into two successive refining hearths, and finally the refined metal is cast as an ingot. The material is contained in water-cooled crucibles but is kept molten by plasma torches or electron beam guns. As the metal flows through the refining hearths, any hard inclusion particles get a chance to dissolve in the surrounding liquid metal or get captured in the "mushy" region between the molten metal and the solid skull on the crucible wall.

4.2. Computational model

The flow and heat transfer in the refining hearth are influenced by buoyancy forces due to density variations and Marangoni forces due to the temperature-dependent surface tension at the surface of the molten pool. The Marangoni forces are quite strong and lead to a significant motion at the free surface. As a result of these forces, the flow is directed from the hot region to the cold region (i.e. away from the plasma torch) and thus helps in pushing the inclusions from the bulk of the liquid to the mushy zone, where they can be captured. The melting/freezing is calculated by using the enthalpy-porosity method of Brent et al. (1988).

4.3. Representative results

The results for the hearth problem have been presented for the plasma hearth in Huang et al. (1999) and for the electron beam hearth in Kelkar et al. (1997). Some sample results are given here. The calculated shape of the liquid pool is shown in Fig. 12. The heating due to the plasma torch has to be such that the resulting pool gives sufficient residence time for the inclusions to dissolve, provides enough solid skull and mushy regions for the inclusions to get trapped, and leaves the inlet and outlet regions unfrozen for an unimpeded flow through the hearth. Fig. 13 shows the distributions of temperature and velocity vectors on selected planes in the refining hearth. Based on the calculated flow field, trajectories of inclusion particles of various sizes and densities can be obtained and their fate determined in terms of dissolution, mushy-zone entrapment, or (the undesirable outcome of) passage into the cast ingot. The results for the particle trajectories are presented in Huang et al. (1999) and Kelkar et al. (1997) for the two types of hearth.

A comparison of predicted and measured pool shapes is shown in Fig. 14. With all the uncertainties in performing the measurements and the necessary simplifications in the computational model for this complex problem, the agreement is quite satisfactory.

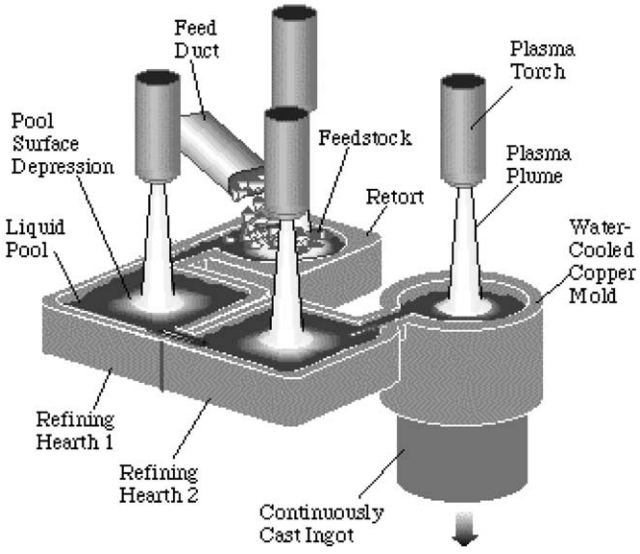

Fig. 11. Schematic diagram for a refining hearth setup.

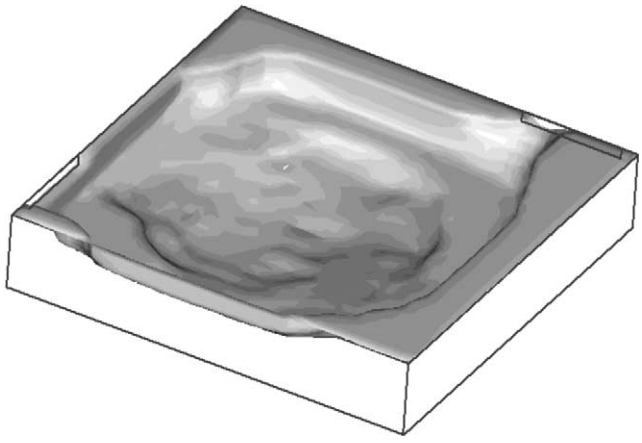

Fig. 12. Calculated pool shape for the refining hearth.

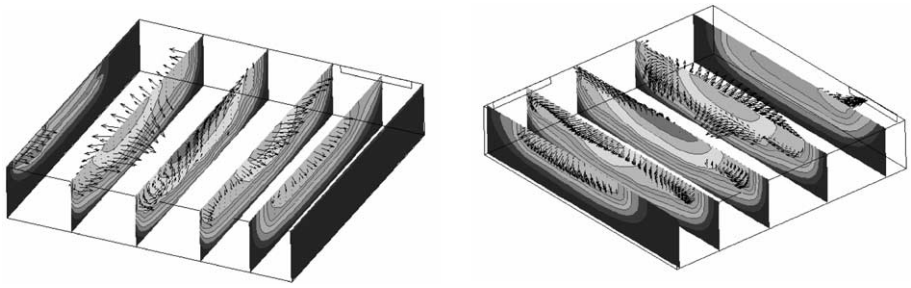

Fig. 13. Temperature fields and velocity vectors in the refining hearth.

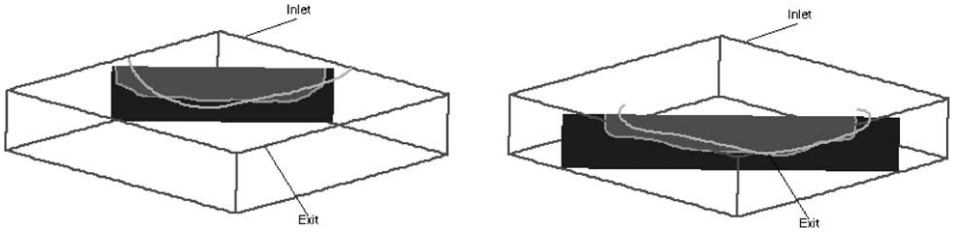

Fig. 14. Comparison of calculated and measured pool shaped in the refining hearth.

5. Cement kiln

5.1. The physical situation

A cement kiln is a chemical reactor designed to convert a solid chemical feed into cement. The heat required for the reactions is supplied by the combustion of coal. Fig. 15 shows a schematic of the kiln. An actual kiln can be 30–200 m long. The axis of the kiln is slightly inclined to the horizontal and the kiln has a slow rotary motion at about 1 rpm. A number of complex chemical reactions take place in the feed bed. The flame due to the combustion of coal is formed in the space above the feed bed as shown. Whereas the feed material travels from left to right, the combustion gases move in the opposite direction. This creates a counter-flow type heat exchange.

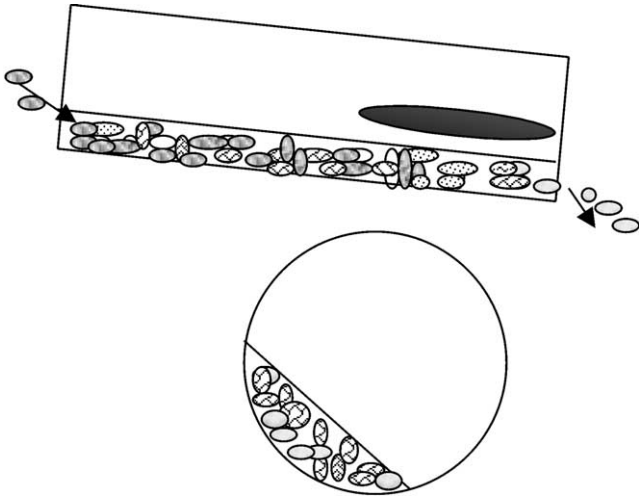

Fig. 15. Schematic of the cement kiln showing the feed bed and the flame.

5.2. The computational model

The coal combustion is handled by calculating trajectories of the coal particles as they give off their volatile hydrocarbons. The hydrocarbons subsequently react with air in gas-phase combustion. The feed bed has an effective thermal conductivity and exchanges heat with the gas flow by convection and radiation. The exothermic and endothermic reactions in the feed bed give rise to appropriate energy sources and sinks. Further details of the model and the results of the simulation are given in Karki et al. (2000a,b).

5.3. Computed results

Fig. 16 shows the distribution of the temperature for the central plane. The hot flame created by the combustion of coal and the cold feed entering the kiln can be clearly seen. As the feed moves through the kiln, it heats up both by heat exchange with the flame and by the internal chemical reactions. A more complete distribution of temperature is displayed in Fig. 17; the direction of the feed movement is away from the observer.

As the combustion proceeds, a large amount of CO is first formed; it subsequently converts to CO_2 and the CO concentration goes down. This behavior can be seen in Fig. 18, where the distribution of CO concentration on the central plane is shown. The axial variations of the

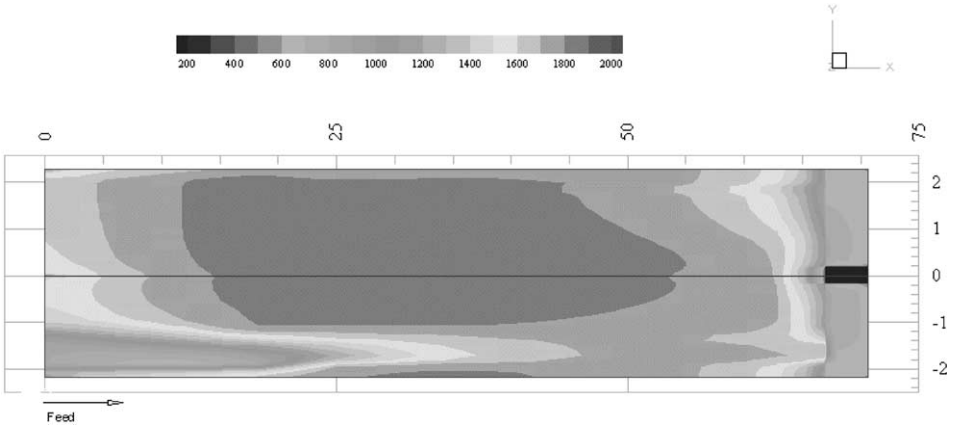

Fig. 16. Temperature distribution on the central plane of the cement kiln.

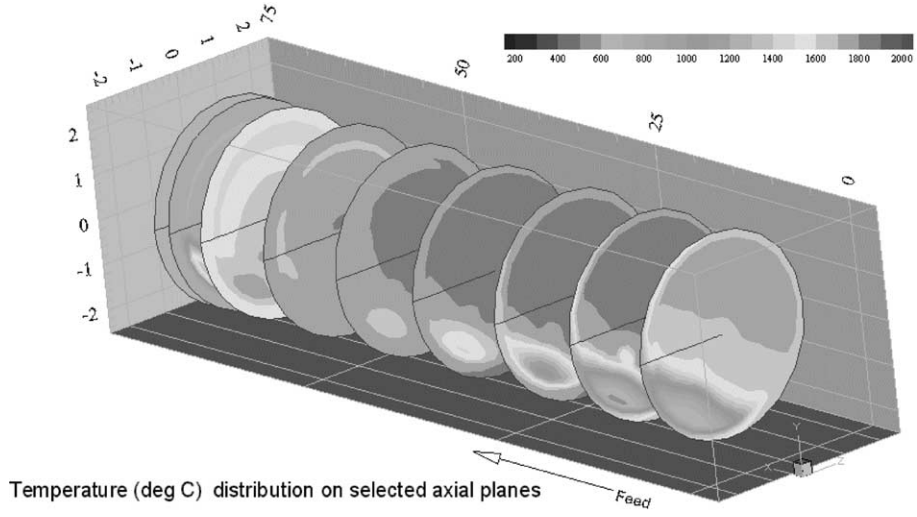

Fig. 17. Temperature distribution on several planes in the cement kiln.

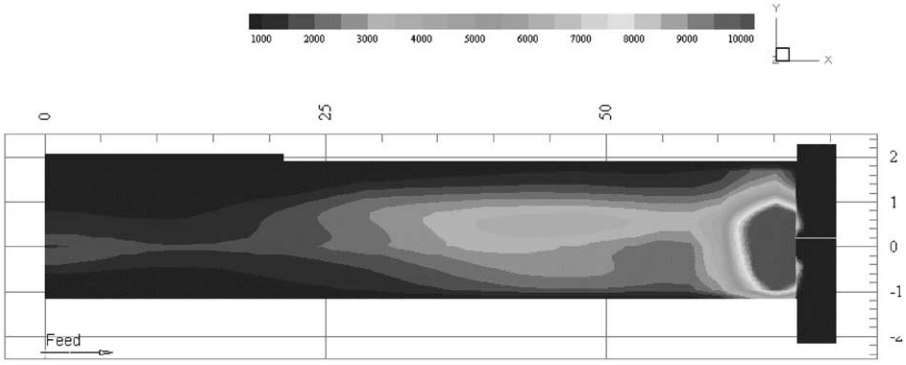

Fig. 18. Distribution of the CO concentration in ppm on the central plane of the cement kiln.

temperatures of the gas and the feed bed are presented in Fig. 19. The conversion of the feed material into cement depends on acquiring the right temperatures for the chemical reactions to occur. A simulation such as this allows the examination of the effect of different parameters on the temperature distribution.

6. Closing remarks

Computational modeling of complex fluid flow and heat transfer has been described for four physical situations of practical interest. Each application involves a number of noteworthy computational and physical as-

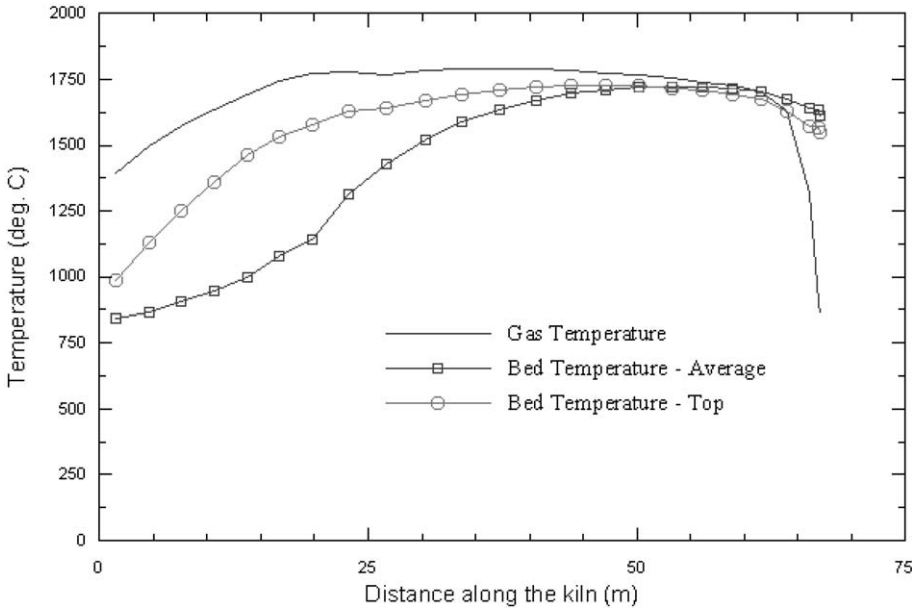

Fig. 19. Axial variation of the temperature of the feed bed and of the gas.

pects. The computational models have been devised to capture the important physical processes and to minimize the computational effort. The results reveal many interesting physical effects and give satisfactory agreement with measurements.

References

Brent, A.D., Voller, V.R., Reid, K.J., 1988. Enthalpy-porosity technique for modeling convection-diffusion phase change: Application to melting of a pure metal. Numerical Heat Transfer 13, 297–318.

Huang, X., Chou, J.S., Pang, Y., 1999. Modeling of plasma arc cold hearth melting and refining of Ti alloys. Proceedings of the 1999 International Symposium on Liquid Metal Processing and Casting, pp. 224–243.

Karki, K.C., Patankar, S.V., Grant, J., 2000. Simulation of fluid flow, combustion, and heat transfer in a coal-fired cement kiln, in: Presser, C., Gupta, A.K. (Eds.), Combustion, Fire, and Computational Modeling of Industrial Combustion Systems, ASME FACT-vol. 23/ASME HTD-vol. 367, pp. 103–114 (2000 ASME International Mechanical Engineering Congress and Exhibition, Orlando, FL, USA).

Karki, K.C., Rosenbluth, E., Patankar, S.V., Levy, S., 2000. CFD model for jet fan ventilation systems, in: 10th Symposium on Aerodynamics and Ventilation of Vehicle Tunnels, BHR Group 2000 Vehicle Tunnels, pp. 355–380.

Kelkar, K.M., Patankar, S.V., Srivatsa, S.K., 1997. Mathematical modeling of the electron beam cold hearth refining of titanium alloys, in: Proceedings of the Electron Beam Melting and Refining Conference, State of the Art 1997, pp. 238–251.

Massachusetts Highway Department and Bechtel/Parsons Brinckerhoff. 1995. Memorial Tunnel Fire Test Ventilation Program, Test Report.

Massachusetts Highway Department/Federal Highway Administration. 1999. Memorial Tunnel Fire Ventilation Test Program, Phase IV Report.